

Research



Article submitted to journal

Subject Areas:

electromagnetic properties,
polycrystalline materials, sea ice

Keywords:

Polycrystals, composites, effective
properties, sea ice

Author for correspondence:

Kenneth M. Golden

e-mail: golden@math.utah.edu

Bounds on the Complex Permittivity of Polycrystalline Materials by Analytic Continuation

A. Gully^{1,2}, J. Lin³, E. Cherkaev¹, and
K. M. Golden¹

¹Department of Mathematics, Univ. of Utah, 155 S
1400 E RM 233, Salt Lake City, UT 84112-0090, USA.

²Department of Mathematics and Statistics, McMaster
Univ., 1280 Main St. West, Hamilton, ON L8S4L8, CA.

³Department of Mathematics, California Polytechnic
State Univ., San Luis Obispo, CA 93407-0403, USA.

An analytic continuation method for obtaining rigorous bounds on the effective complex permittivity of polycrystalline composite materials is developed. It is assumed that the composite consists of many identical anisotropic crystals, each with a unique orientation. The key step in obtaining the bounds involves deriving an integral representation for the effective complex permittivity, which separates parameter information from geometrical information. First and second order forward bounds are then found using knowledge of the single crystal complex permittivity tensor and the mean crystal orientation. Inverse bounds are also developed, which recover information about the mean single crystal orientation from the effective complex permittivity of the material. We then apply the polycrystalline bounds to sea ice, a critical component of the climate system. Different ice types, which result from different growth conditions, have different single crystal orientation and size statistics. These characteristics can dramatically change the fluid transport properties of sea ice, which control many geophysical and biogeochemical processes important to the climate and polar ecosystems. We obtain the bounds for sea ice through two-scale homogenization, where the single crystal tensor is obtained numerically and then incorporated into the analytic continuation procedure. The forward bounds are compared with columnar sea ice data and are found to be in excellent agreement. Further, the inverse bounds are applied to sea ice as well, helping to lay the groundwork for determining ice type using remote sensing techniques.

1. Introduction

A polycrystalline composite material consists of many single crystals that can vary in shape, size, and orientation. A broad range of manufactured and naturally occurring materials are polycrystalline, including metals, ceramics, rocks, glacial ice, and sea ice. Here we consider the electromagnetic behavior of polycrystalline media when the wavelength is much larger than the scale of the underlying microstructure of the composite. When in this regime, the quasistatic approximation is valid, and the electric and displacement fields can be viewed at time-independent fields. Then the polycrystalline composite can be characterized electromagnetically via the effective complex permittivity tensor ϵ^* .

The macroscopic permittivity or dielectric tensor ϵ^* of a polycrystalline composite depends directly on its microstructural properties, such as the complex permittivity tensor of the individual crystals and their microstructural geometry, i.e., how the crystals are oriented. Due to the complicated nature of the microstructure, explicitly calculating ϵ^* is highly non-trivial, and can generally only be accomplished if the exact microstructure is known and with the assistance of very powerful numerical computations. Therefore, using partial microstructural information that may be available to estimate or bound ϵ^* is a very practical and useful approach.

There has been extensive work in the past on estimating and bounding ϵ^* for composite materials. The books by Cherkaev [8] and Milton [38] thoroughly discuss much of this work. In particular, ϵ^* has been intensively studied for two phase composites. Rigorous bounds were first obtained in the early 1980's using the analytic continuation method, where the effective parameter is treated as an analytic function of the ratio of the component parameters [5,17,35]. These bounds assume that the complex permittivity of each component is known and that there is some partial information available about the microstructure. The most general bounds assume only knowledge of the relative volume fractions of each material, resulting in the complex versions of the classical arithmetic and harmonic mean bounds for a two-component material. Tighter bounds can be found when more geometrical information is available, such as knowing the that microstructure is isotropic [25], or that the composite has a *matrix-particle* structure [44], etc.

Additionally, the electromagnetic response of a composite material can be used to help determine microstructural properties when approached as an inverse problem. That is, given information on ϵ^* , different microstructural details be resolved, such as the relative volume fractions of each component of the material. This has also been extensively investigated for a two-component composite [9,10,21,33,34,40,53], and inverse bounds have been developed.

For some composite structures, it is more appropriate to assume that the material consists of many identical anisotropic pieces that are oriented in different directions. This is the case for a polycrystalline composite. Polycrystalline materials have been studied for decades, and in particular, there has been a significant amount of work done on bounding the effective (real) conductivity [2,8,11,12,26,27,36–39,45,46]. The books by Cherkaev [8] and Milton [38] discuss the majority of this work.

Here we develop an analytic continuation method for obtaining complex bounds on ϵ^* for a three-dimensional (transversely isotropic, or uniaxial) polycrystalline composite material. The key step in obtaining the bounds involves deriving an integral representation for the effective complex permittivity tensor, which separates parameter information from geometrical information. By making an assumption about the complex permittivity tensor of each individual crystal and assuming some knowledge about the mean single crystal orientation, we obtain first order polycrystalline bounds on ϵ^* for the entire polycrystal. If we further assume the polycrystalline material has the “polycrystalline Hashin-Shtrikman condition” [38], which is essentially geometric isotropy, second order forward bounds are found. Further, we then use a method similar to that in [9], and derive inverse bounds for a polycrystal. Thus, knowing ϵ^* and the complex permittivity tensor of an individual crystal, we will bound the mean single crystal orientation.

As a demonstration of the complex polycrystalline bounds, we compare them to sea ice data. Investigating the electromagnetic behavior of sea ice is not only interesting from a composite material point of view, but also because of the valuable information that can be recovered using remote sensing techniques, such as sea ice thickness and fluid transport properties. Sea ice covers between 7-10% of the earth's ocean surface and is both an indicator and agent of climate change [47,52,54]. Since the 1980's there has been a steady decline in Arctic summer sea ice extent, with a much more rapid decline over the past decade [41]. During the winter months in the Arctic and Antarctic, the extensive sea ice packs serve as the boundary layer which mediates the exchange of heat, moisture, and momentum between the atmosphere and ocean [28,52]. The vast expanses of sea ice also serve as a habitat for rich microbial communities living in the brine microstructure of porous sea ice [15,29,52]. In turn, these microbial communities are primary providers for the complex food webs in the polar oceans.

Due to the global nature of monitoring the earth's sea ice packs, large scale information is usually obtained via remote sensing from platforms on satellites, aircraft and ships [7,21,30,48,58]. One of the grand challenges of sea ice remote sensing is to accurately recover the thickness distribution of the pack. Assessing the impact of climate change on the polar regions involves monitoring not only the ice extent, but the ice volume, which requires knowledge of ice thickness. Recently there has been increasing interest in using low frequency electromagnetic induction devices to estimate sea ice thickness [42]. In addition to assessing ice thickness, remotely monitoring the fluid transport properties of sea ice is of increasing interest because of the broad range of geophysical and biological processes it mediates in the polar marine environment. For example, the evolution of melt ponds and summer ice albedo is constrained by drainage through porous sea ice [14], where ice-albedo feedback is believed to play a key role in the decline of summer Arctic sea ice [41]. Fluid flow also facilitates snow-ice formation [32], the evolution of the salt budget [52], convection-enhanced thermal transport [31], CO₂ exchange [43], and biomass build-up sustained by nutrient fluxes [15,52]. In a recent study [23], we found evidence that different ice microstructures, such as columnar versus granular, can dramatically change the fluid transport properties of sea ice. Thus, determining ice type using remote sensing techniques may be a particularly useful application.

There has been considerable work in the past on estimating and bounding ϵ^* for sea ice, particularly in the microwave region [1,9,16,16,19,19,20,22,22,24,44,49,50,55,58]. The rigorous two-component bounds mentioned above have successfully been used to bound ϵ^* for sea ice [9,16,19,22,24,44]. These bounds assume that sea ice is a two-component material, consisting of a pure ice and brine phase. The forward bounds recover information on ϵ^* using information about the microstructure, such as brine volume fractions or porosity ϕ (and sometimes further assuming statistical isotropy), while the inverse bounds attempt to recover ϕ from ϵ^* .

Here we apply the first order forward polycrystalline bounds to sea ice. We see a dramatic improvement over the classic two-component bounds, because these new bounds include additional information about single crystal orientations. Here we use the data set presented in [1] to compare the polycrystalline bounds to sea ice. This data set is the same one used in [9,16,44], thus helping provide some continuity between different types of bounds. In addition to providing ϵ^* and ϕ measurements, the data set provides detailed crystallographic data, which will be critical when in applying the bounds. Notationally, we will reserve R_1 and R_2 to indicate the previously reported two-component forward bounds and use R_3 and R_4 to describe the new polycrystalline forward bounds. The single crystal complex permittivity tensor is obtained by numerical simulation using X-ray CT data on sea ice, along with with known brine volume fractions and ice and brine permittivities. Further, the inverse method that we develop is applied to sea ice and we obtain bounds on the mean single crystal orientation. Columnar and granular microstructures have different mean single crystal orientations [56], thus this inverse approach helps lay the groundwork for determining ice type when using remote sensing techniques.

2. Forward Bounds on the Effective Complex Permittivity of a Polycrystalline Material

Consider the constitutive relation $\mathbf{D}(\mathbf{x}, \omega) = \epsilon(\mathbf{x}, \omega) \mathbf{E}(\mathbf{x}, \omega)$, where $\mathbf{D}(\mathbf{x}, \omega)$ and $\mathbf{E}(\mathbf{x}, \omega)$ are stationary random displacement and electric fields and $\epsilon(\mathbf{x}, \omega)$ is the permittivity tensor of some medium. Here $\mathbf{x} \in \mathbb{R}^d$ and $\omega \in \Omega$, where Ω is the set of all realizations of the random medium. Let us consider a polycrystalline material, where each crystal has the same complex permittivity tensor but with different orientation. Thus, we let $\epsilon(\mathbf{x}, \omega) = \mathbf{B}^{-1}(\mathbf{x}, \omega) \epsilon_d \mathbf{B}(\mathbf{x}, \omega)$, where $\mathbf{B}(\mathbf{x}, \omega)$ is a rotation matrix describing the orientation of a crystal at location \mathbf{x} and realization ω , and ϵ_d is the same permittivity tensor for each crystal and can be written

$$\epsilon_d = \begin{bmatrix} \epsilon_1 & 0 & 0 \\ 0 & \epsilon_2 & 0 \\ 0 & 0 & \epsilon_2 \end{bmatrix}.$$

Here, we are assuming that each crystal has the same permittivity value ϵ_2 in both horizontal directions (transversely isotropic or uniaxial) with anisotropy occurring in the vertical direction with permittivity value ϵ_1 . It is assumed that ϵ_1 and ϵ_2 can take complex values. Then making the assumptions that we are in the quasistatic regime and there is no free charge, we can write $\nabla \times \mathbf{E}(\mathbf{x}, \omega) = 0$ and $\nabla \cdot \mathbf{D}(\mathbf{x}, \omega) = 0$. Now, letting $\langle \cdot \rangle$ represent an ensemble average over Ω or a spatial average over all of \mathbb{R}^d , we then write $\langle \mathbf{E}(\mathbf{x}, \omega) \rangle = \mathbf{e}_k$, where \mathbf{e}_k is a unit vector in the k th direction for some $k = 1, \dots, d$. For notational simplicity, we write $\mathbf{E}(\mathbf{x}, \omega) = \mathbf{E}$ and $\mathbf{D}(\mathbf{x}, \omega) = \mathbf{D}$. The effective complex permittivity tensor is then defined via

$$\langle \mathbf{D} \rangle = \epsilon^* \langle \mathbf{E} \rangle. \quad (2.1)$$

From this we can write $[\epsilon^*]_{kk} = \mathbf{e}_k^T \epsilon^* \mathbf{e}_k = \langle \mathbf{e}_k^T \epsilon \mathbf{e}_k \rangle$ and then define $\epsilon^* = [\epsilon^*]_{kk}$. This allows us to strictly examine the kk th component of the effective permittivity tensor and simplifies the notation. Thus, we can rewrite the equation as $\epsilon^* = \langle \mathbf{e}_k^T \mathbf{B}^{-1} \epsilon_d \mathbf{B} \mathbf{e}_k \rangle$. Due to the homogeneity of the effective parameters $\epsilon^*(\lambda \epsilon_1, \lambda \epsilon_2) = \lambda \epsilon^*(\epsilon_1, \epsilon_2)$, ϵ^* only depends on the ratio $h = \epsilon_1 / \epsilon_2$ and we define $m(h) = \epsilon^* / \epsilon_2$. Therefore, we have the equation

$$m(h) = \frac{\epsilon^*}{\epsilon_2} = \langle \mathbf{e}_k^T \mathbf{B}^{-1} \begin{bmatrix} h & 0 & 0 \\ 0 & 1 & 0 \\ 0 & 0 & 1 \end{bmatrix} \mathbf{B} \mathbf{e}_k \rangle.$$

Notice that this is equivalent to

$$m(h) = \langle \mathbf{e}_k^T (\mathbf{I} - (1 - h) \mathbf{B}^{-1} \mathbf{C} \mathbf{B}) \mathbf{e}_k \rangle$$

where $\mathbf{C} = \mathbf{e}_1(\mathbf{e}_1)^T$, \mathbf{I} is a 3x3 identity matrix, and \mathbf{e}_1 is a unit vector in the first direction [3,38]. To simplify the notation, we define $\mathbf{R} = \mathbf{B}^{-1} \mathbf{C} \mathbf{B}$, and can then write $m(h) = \langle \mathbf{e}_k^T (\mathbf{I} - (1 - h) \mathbf{R}) \mathbf{e}_k \rangle$.

The two main properties of $m(h)$ are that it is analytic off $(-\infty, 0]$ in the h -plane, and that it maps the upper half plane to the upper half plane [4,17], so that it is an example of a Herglotz or Stieltjes function. The key step for obtaining forward bounds is to use an analytic continuation method which involves obtaining an integral representation for ϵ^* . If we let $s = 1/(1 - h)$, then we can define

$$F(s) = 1 - m(h) = 1 - \epsilon^* / \epsilon_2 = \langle (s^{-1} \mathbf{e}_k^T \mathbf{R} \mathbf{e}_k) \rangle.$$

From here, we must now obtain a resolvent representation for \mathbf{E} , which will allow us to find an integral representation for $F(s)$.

To find the resolvent representation of \mathbf{E} , first examine $\nabla \cdot \mathbf{D} = 0$, which implies that $\nabla \cdot \epsilon \mathbf{E} = 0$. Then, let \mathbf{G} be a vector representing the mean fluctuations in the electric field and call $\mathbf{E} = \mathbf{e}_k + \mathbf{G}$. Expand ϵ and \mathbf{E} using the previous definitions and formulate the equation

$$\nabla \cdot (\mathbf{I} - s^{-1}\mathbf{R})(\mathbf{e}_k + \mathbf{G}) = 0, \quad (2.2)$$

where \mathbf{I} is again a 3x3 identity matrix. After multiple algebraic manipulations, one can obtain the equation

$$s\mathbf{G} + \nabla(-\Delta)^{-1}\nabla \cdot (\mathbf{R}\mathbf{E}) = 0. \quad (2.3)$$

Now, define the operator $\nabla(-\Delta)^{-1}\nabla = \mathbf{\Gamma}$, which is the same gamma in [16,17,19,24], and find the resolvent representation for \mathbf{E} to be

$$\mathbf{E} = s[\mathbf{I} + \mathbf{\Gamma}\mathbf{R}]^{-1}\mathbf{e}_k. \quad (2.4)$$

Using this resolvent representation to express $F(s)$, one finds the equation

$$F(s) = \langle \mathbf{e}_k^T \mathbf{R}(s\mathbf{I} + \mathbf{\Gamma}\mathbf{R})^{-1} \mathbf{e}_k \rangle. \quad (2.5)$$

Using the spectral representation theorem $F(s)$ takes the particularly nice form

$$F(s) = \int_0^1 \frac{d\mu(z)}{s - z}, \quad (2.6)$$

where the positive measure μ on $[0, 1]$ is the spectral measure of the self-adjoint operator $\mathbf{\Gamma}\mathbf{R}$. $F(s)$ is also analytic off $[0, 1]$ in the s -plane, which is the only restriction for this integral representation. All of the geometrical information is now contained inside of μ and all of the parameter information is contained in s , including the electromagnetic wave frequency. Expanding $F(s)$, we find

$$F(s) = \langle \mathbf{e}_k^T \mathbf{R} \mathbf{e}_k \rangle / s + \langle \mathbf{e}_k^T \mathbf{R} \mathbf{\Gamma} \mathbf{R} \mathbf{e}_k \rangle / s^2 + \dots, \quad (2.7)$$

$$F(s) = \mu_0 / s + \mu_1 / s^2 + \dots \quad (2.8)$$

Thus, statistical assumptions about the geometry that are incorporated into μ via its moments $\mu_n = \int_0^1 z^n d\mu(z)$, can be calculated from the correlation functions of the random medium, with $\mu_n = (-1)^n \langle \mathbf{e}_k^T \mathbf{R} [(\mathbf{\Gamma}\mathbf{R})^n \mathbf{e}_k] \rangle$. For the complex elementary bounds it is assumed that we know only $\mu_0 = \langle \mathbf{e}_k^T \mathbf{R} \mathbf{e}_k \rangle$. This quantity can be easily and quickly calculated provided we know the dimension of the composite and crystal orientation statistics. A calculation of this will be done when the bounds are compared to actual sea ice data in section 4. The statistical average $\langle \mathbf{e}_k^T \mathbf{R} \mathbf{e}_k \rangle$ can be thought of as the “mean orientation,” or as the percentage of the single crystals in the k th direction.

Bounds on ϵ^* , or $F(s)$, are obtained by fixing s in (2.6), varying over admissible measures μ (or admissible geometries), such as those that satisfy only $\mu_0 = \langle \mathbf{e}_k^T \mathbf{R} \mathbf{e}_k \rangle$, and finding the corresponding range of values of $F(s)$ in the complex plane [17]. The bound R_3 assumes only that the mean crystal orientation $\langle \mathbf{e}_k^T \mathbf{R} \mathbf{e}_k \rangle$ of the single crystals is known, with $\mu_0 = \langle \mathbf{e}_k^T \mathbf{R} \mathbf{e}_k \rangle$ satisfied. In this case, the admissible set of measures form a compact, convex set \mathcal{M}_0 . Since (2.6) is a linear functional of μ , the extreme values of F are attained by extreme points of \mathcal{M}_0 , which are the Dirac point measures $\langle \mathbf{e}_k^T \mathbf{R} \mathbf{e}_k \rangle \delta z$. The values of ϵ^* lie inside the region R_3 bounded by circular arcs, one of which is parameterized in the F -plane by

$$C_3(z) = \frac{\langle \mathbf{e}_k^T \mathbf{R} \mathbf{e}_k \rangle}{s - z}, \quad -\infty \leq z \leq \infty. \quad (2.9)$$

To display the other arc, we use the auxiliary function [6] $E(s) = 1 - \epsilon_1 / \epsilon^*$, which is a Herglotz function like $F(s)$, analytic off $[0, 1]$. Then in the E -plane, we can parameterize the other circular

boundary of R_3 by

$$\hat{C}_3(z) = \frac{1 - \langle \mathbf{e}_k^T \mathbf{R} \mathbf{e}_k \rangle}{s - z}, \quad -\infty \leq z \leq \infty. \quad (2.10)$$

In the common ϵ^* -plane, R_3 takes the following form for the “lower” and “upper” bounds, which are still circular arcs, ϵ_l^* and ϵ_u^* , respectively.

$$\epsilon_u^*(z) = \epsilon_2 - \epsilon_2 \left(\frac{\langle \mathbf{e}_k^T \mathbf{R} \mathbf{e}_k \rangle}{s - z} \right), \quad -\infty \leq z \leq \infty. \quad (2.11)$$

$$\epsilon_l^*(z) = \epsilon_1 \left(1 - \frac{1 - \langle \mathbf{e}_k^T \mathbf{R} \mathbf{e}_k \rangle}{s - z} \right)^{-1}, \quad -\infty \leq z \leq \infty. \quad (2.12)$$

When ϵ_1 and ϵ_2 are real and positive, the bounds collapse to the interval

$$1/(\langle \mathbf{e}_k^T \mathbf{R} \mathbf{e}_k \rangle / \epsilon_1 + (1 - \langle \mathbf{e}_k^T \mathbf{R} \mathbf{e}_k \rangle) / \epsilon_2) \leq \epsilon^* \leq \langle \mathbf{e}_k^T \mathbf{R} \mathbf{e}_k \rangle \epsilon_1 + (1 - \langle \mathbf{e}_k^T \mathbf{R} \mathbf{e}_k \rangle) \epsilon_2.$$

These are the analogous arithmetic (upper) and harmonic (lower) mean bounds for a polycrystalline material in the single direction k .

To obtain second order complex bounds further assumptions need to be made. For instance, if the polycrystalline composite is assumed to have the “polycrystalline Hashin-Shtrikman condition” [38] or essentially geometric isotropy, then $\mu_1 = -\langle \mathbf{e}_k^T \mathbf{R} \mathbf{I} \mathbf{R} \mathbf{e}_k \rangle = (d - 1)/d^3$, where d is the dimension of the polycrystalline composite. In two dimensions, we define a polycrystalline material to be geometrically isotropic if for every crystal in the polycrystalline composite with orientation off the vertical direction described by the normalized vector $\langle x, y \rangle$, there exist three other crystals that have orientations $\langle x, -y \rangle$, $\langle y, x \rangle$, and $\langle y, -x \rangle$. A similar definition can be made for three dimensions, where groups of 24 crystals are needed instead of groups of four. (Note: Several special examples in two dimensions where only groups of two are required include polycrystalline materials where all the single crystals are vertically and horizontally aligned or all the single crystals have an orientation angle of $\pm\pi/4$ radians or ± 45 degrees off the vertical axis. In a similar fashion, if all the single crystals are vertically or horizontally aligned in three dimensions, only groups of three crystals are required.)

Here we show the derivation for the value of $\mu_1 = -\langle \mathbf{e}_k^T \mathbf{R} \mathbf{I} \mathbf{R} \mathbf{e}_k \rangle$ for two dimensions. (An analogous argument can be demonstrated for three dimensions.) Recall that $\mathbf{I} = \nabla(-\Delta)^{-1} \nabla \cdot$ and define $(-\Delta)^{-1}$ in terms of a Green’s function so that $((-\Delta)^{-1} f)(x) = \int_{\mathbb{R}^d} g(x, y) f(y) dy$, where $\Delta g(x) = -\delta_y(x)$. Therefore, we can write

$$\mu_1 = \langle \mathbf{e}_k^T \mathbf{R} \nabla \int_{\mathbb{R}^d} g(x, y) \nabla \cdot \mathbf{R} \mathbf{e}_k dy \rangle, \quad (2.13)$$

where in two dimensions \mathbf{R} takes the form

$$\mathbf{R} = \begin{bmatrix} \cos^2(\theta) & -\cos(\theta)\sin(\theta) \\ -\cos(\theta)\sin(\theta) & \sin^2(\theta) \end{bmatrix} = \begin{bmatrix} a & -b \\ -b & c \end{bmatrix},$$

where for notation simplicity define $a = \cos^2(\theta)$, $-b = -\cos(\theta)\sin(\theta)$, and $c = \sin^2(\theta)$, where θ is the angle of orientation off the vertical axis. Define $\tilde{\mathbf{R}} = \mathbf{R} - \mathbf{I}(\langle \mathbf{e}_1^T \mathbf{R} \mathbf{e}_1 \rangle, \langle \mathbf{e}_2^T \mathbf{R} \mathbf{e}_2 \rangle)^T$, which is translationally invariant, and then under the divergence theorem we can write

$$\begin{aligned} \mu_1 &= \langle -\mathbf{e}_k^T \mathbf{R} \nabla \int_{\mathbb{R}^d} (\nabla g(x, y)) \cdot \mathbf{R} \mathbf{e}_k dy \\ &\quad - \mathbf{e}_k^T \mathbf{R} \nabla \int_{\mathbb{R}^d} (\nabla g(x, y)) \cdot \mathbf{I}(\langle \mathbf{e}_1^T \mathbf{R} \mathbf{e}_1 \rangle, \langle \mathbf{e}_2^T \mathbf{R} \mathbf{e}_2 \rangle)^T \mathbf{e}_k dy \\ &\quad + \mathbf{e}_k^T \mathbf{R} \nabla \int_{\partial \mathbb{R}} (g(x, y) \tilde{\mathbf{R}} \mathbf{e}_k) \cdot n dA \rangle. \end{aligned} \quad (2.14)$$

***** What does $\int_{\partial \mathbb{R}}$ mean?

Again for simplicity, let us consider the terms separately. The intent here is to find crystal orientation combinations so that the Laplacian operator is recovered, and together with $g(x, y)$ we obtain a delta function inside the integral, or for the term to become zero. Examining the first term, analyzing the first direction ($k = 1$), and using the notation $D_x = d/dx$, we see that

$$-\mathbf{e}_1^T \mathbf{R} \nabla \int_{\mathbb{R}^d} (\nabla g(x, y)) \cdot \mathbf{R} \mathbf{e}_1 dy = \int_{\mathbb{R}^d} (a^2 D_{xx} - 2ab D_{xy} + b^2 D_{yy}) g(x, y) dy. \quad (2.15)$$

A similar result is found when examining the second direction,

$$-\mathbf{e}_2^T \mathbf{R} \nabla \int_{\mathbb{R}^d} (\nabla g(x, y)) \cdot \mathbf{R} \mathbf{e}_2 dy = \int_{\mathbb{R}^d} (b^2 D_{xx} - 2bc D_{xy} + c^2 D_{yy}) g(x, y) dy. \quad (2.16)$$

Together, these describe the vertical and horizontal components of a single crystal inside a statistical average. If we now impose the condition that the vertical and horizontal components have the same statistical average for a single crystal, we observe that

$$\langle -\mathbf{e}_k^T \mathbf{R} \nabla \int_{\mathbb{R}^d} (\nabla g(x, y)) \cdot \mathbf{R} \mathbf{e}_k dy \rangle = 1/d \langle \int_{\mathbb{R}^d} [(a^2 + b^2) D_{xx} - 2(ab + bc) D_{xy} + (b^2 + c^2) D_{yy}] g(x, y) dy \rangle. \quad (2.17)$$

Thus, for the term $[(a^2 + b^2) D_{xx} - 2(ab + bc) D_{xy} + (b^2 + c^2) D_{yy}]$ to become the Laplacian operator, $a^2 = c^2$ and $b = 0$. This is equivalent to every crystal in the polycrystalline material having either perfect vertical or horizontal rotations with an equal amount of crystals in the vertical direction and horizontal direction. Therefore, $\langle -\mathbf{e}_k^T \mathbf{R} \nabla \int_{\mathbb{R}^d} (\nabla g(x, y)) \cdot \mathbf{R} \mathbf{e}_k dy \rangle = 1/d^2$.

This same line of reasoning can be expanded into a geometrically isotropic polycrystalline material. That is, let us now consider “groups” of four single crystals under the statistical average. If four crystals are examined at once, the condition for recovering the Laplacian operator becomes

$$\begin{aligned} & (a_1^2 + a_2^2 + a_3^2 + a_4^2 + b_1^2 + b_2^2 + b_3^2 + b_4^2) D_{xx} \\ & - 2(a_1 b_1 + a_2 b_2 + a_3 b_3 + a_4 b_4 + b_1 c_1 + b_2 c_2 + b_3 c_3 + b_4 c_4) D_{xy} \\ & + (b_1^2 + b_2^2 + b_3^2 + b_4^2 + c_1^2 + c_2^2 + c_3^2 + c_4^2) D_{yy} = q(D_{xx} + D_{yy}), \end{aligned} \quad (2.18)$$

where q is some constant. Thus, $a_1^2 + a_2^2 + a_3^2 + a_4^2 = c_1^2 + c_2^2 + c_3^2 + c_4^2$ and $a_1 b_1 + a_2 b_2 + a_3 b_3 + a_4 b_4 + b_1 c_1 + b_2 c_2 + b_3 c_3 + b_4 c_4 = 0$. These conditions are satisfied provided that the orientation off the vertical directions for the four crystals, in terms of normalized vectors are $\langle x, y \rangle$, $\langle x, -y \rangle$, $\langle y, -x \rangle$, and $\langle y, x \rangle$. Conveniently, for these four specific crystals, q takes the value of $q = 1/d$. Therefore, the same result holds for the statistical average as before and we see that

$$\langle -\mathbf{e}_k^T \mathbf{R} \nabla \int_{\mathbb{R}^d} (\nabla g(x, y)) \cdot \mathbf{R} \mathbf{e}_k dy \rangle = 1/d^2. \quad (2.19)$$

Now consider the second term from equation 2.14, which is $-\mathbf{e}_k^T \mathbf{R} \nabla \int_{\mathbb{R}^d} (\nabla g(x, y)) \cdot \mathbf{I}(\langle \mathbf{e}_1^T \mathbf{R} \mathbf{e}_1 \rangle, \langle \mathbf{e}_2^T \mathbf{R} \mathbf{e}_2 \rangle)^T \mathbf{e}_k dy$. Similar to the technique applied above, if we consider a group of four crystals and examine the vertical and horizontal components (i.e., $k = 1, 2$), then over the statistical average

$$\begin{aligned} & \langle -\mathbf{e}_k^T \mathbf{R} \nabla \int_{\mathbb{R}^d} (\nabla g(x, y)) \cdot \mathbf{I}(\langle \mathbf{e}_1^T \mathbf{R} \mathbf{e}_1 \rangle, \langle \mathbf{e}_2^T \mathbf{R} \mathbf{e}_2 \rangle)^T \mathbf{e}_k dy \rangle \\ & = 1/d \langle \langle \mathbf{e}_1^T \mathbf{R} \mathbf{e}_1 \rangle \int_{\mathbb{R}^d} [(a_1 + a_2 + a_3 + a_4) D_{xx} - (b_1 + b_2 + b_3 + b_4) D_{xy}] g(x, y) dy \rangle \\ & \quad + \langle \mathbf{e}_2^T \mathbf{R} \mathbf{e}_2 \rangle \int_{\mathbb{R}^d} [(c_1 + c_2 + c_3 + c_4) D_{yy} - (b_1 + b_2 + b_3 + b_4) D_{xy}] g(x, y) dy \rangle. \end{aligned} \quad (2.20)$$

If geometric isotropy as defined above is assumed, then $\langle \mathbf{e}_1^T \mathbf{R} \mathbf{e}_1 \rangle = \langle \mathbf{e}_2^T \mathbf{R} \mathbf{e}_2 \rangle$, $a_1 + a_2 + a_3 + a_4 = c_1 + c_2 + c_3 + c_4$, and $b_1 + b_2 + b_3 + b_4 = 0$. Therefore, the second term also introduces a Laplacian operator and we see that

$$\langle -\mathbf{e}_k^T \mathbf{R} \nabla \int_{\mathbb{R}^d} (\nabla g(x, y)) \cdot \mathbf{I}(\langle \mathbf{e}_1^T \mathbf{R} \mathbf{e}_1 \rangle, \langle \mathbf{e}_2^T \mathbf{R} \mathbf{e}_2 \rangle)^T \mathbf{e}_k dy \rangle = (1/d)(1/d)(1/d). \quad (2.21)$$

Finally, consider the third term from equation 2.14, which is $\mathbf{e}_k^T \mathbf{R} \nabla \int_{\partial \mathbb{R}} (g(x, y) \tilde{\mathbf{R}} \mathbf{e}_k) \cdot ndA$. Here, we see that if we consider the same group of four crystals as above that are geometrically isotropic, and under the statistical average,

$$\begin{aligned} & \langle \mathbf{e}_k^T \mathbf{R} \nabla \int_{\partial \mathbb{R}} (g(x, y) \tilde{\mathbf{R}} \mathbf{e}_k) \cdot ndA \rangle \\ &= (1/d) \langle \left(\int_{\partial \mathbb{R}} [(a_1^2 + a_2^2 + a_3^2 + a_4^2 + b_1^2 + b_2^2 + b_3^2 + b_4^2) D_x \right. \\ & \quad + (-a_1 b_1 - a_2 b_2 - a_3 b_3 - a_4 b_4 - b_1 c_1 - b_2 c_2 - b_3 c_3 - b_4 c_4) D_y, \\ & \quad (-a_1 b_1 - a_2 b_2 - a_3 b_3 - a_4 b_4 - b_1 c_1 - b_2 c_2 - b_3 c_3 - b_4 c_4) D_x \\ & \quad \left. + (c_1^2 + c_2^2 + c_3^2 + c_4^2 + b_1^2 + b_2^2 + b_3^2 + b_4^2) D_y] \right)^T \cdot ndA \\ & \quad - \int_{\partial \mathbb{R}} (1/d) [(a_1 + a_2 + a_3 + a_4) D_x + (-b_1 - b_2 - b_3 - b_4) D_y, \\ & \quad (-b_1 - b_2 - b_3 - b_4) D_x + (c_1 + c_2 + c_3 + c_4) D_y]^T \cdot ndA \rangle = 0. \end{aligned} \quad (2.22)$$

Putting all of this together, we see that μ_1 in equation 2.14, under the assumption of geometrical isotropy, satisfies

$$\mu_1 = (1/d)[(1/d) - (1/d)(1/d)] = \frac{d-1}{d^3}. \quad (2.23)$$

This value for μ_1 is analogous to the $\mu_1 = (1/d)[p_1 - p_1^2]$ value found for a two-component material in [17].

Thus, if the polycrystalline material is further assumed to have the Hashin-Shtrikman condition, then $F(s)$ is known to second order, with $\mu_0 = 1/d$ and $\mu_1 = (d-1)/d^3$, so that

$$F(s) = 1/(sd) + (d-1)/(s^2 d^3). \quad (2.24)$$

A convenient transform $F_1(s) = 1/(\langle \mathbf{e}_k^T \mathbf{R} \mathbf{e}_k \rangle) - 1/sF(s)$ allows for this information to be included. It is known [18] that $F_1(s)$ is an upper half plane function analytic off $[0, 1]$ and has the representation

$$F_1(s) = \int_0^1 \frac{d\mu_1(z)}{s-z}, \quad (2.25)$$

Under the additional assumption of geometric isotropy $F_1(s)$ is known only to first order, where $F_1(s) = (d-1)/(ds) + \dots$, and $\mu_1^0 = (d-1)/(ds)$. Thus the values of $F_1(s)$ lie in the circular arc $(d-1)/[(d)(s-z)]$, $-\infty \leq z \leq \infty$. Mapping this arc back into the F -plane, we can parameterize one boundary of R_4 by

$$C_4(z) = \frac{(1/d)(s-z)}{s(s-z - \frac{d-1}{d^2})}, \quad -\infty \leq z \leq \infty. \quad (2.26)$$

Similarly, to display the other arc, we use the auxiliary function $E(s) = 1 - \epsilon_1/\epsilon^* = (1 - sF(s))/(s(1 - F(s)))$, and find that $E(s) = (d-1)/(ds) + (d^2 - 2d - 1)/(d^3 s^2)$. Again, using a similar method as with $F(s)$, an arc can be found in the E -plane, and we can parameterize the

other circular boundary of R_4 by

$$\hat{C}_4(z) = \frac{((d-1)/d)(s-z)}{s(s-z - \frac{d-1}{d^2})}, \quad -\infty \leq z \leq \infty. \quad (2.27)$$

When ϵ_1 and ϵ_2 are real and positive, the bounds collapse to the interval

$$\epsilon_2(1 - 1/(ds - [d-1]/d)) \leq \epsilon^* \leq \epsilon_1/(1 - [(d-1)/(ds - [d-1]/d)]), \quad (2.28)$$

where $s = \epsilon_2/(\epsilon_2 - \epsilon_1)$ and $\epsilon_2 \leq \epsilon_1$. These are exactly the Hashin-Shtrikman bounds for an isotropic polycrystalline composite [26]. Further, if we evaluate the two-dimensional second order complex forward bounds for a two-component material [5,17,35], where each material has a volume fraction of 50%, we see that they are in agreement with the two dimensional second order complex forward polycrystalline bounds. The three-dimensional bounds are also in agreement.

For the purpose of comparing these bounds to previously established ones on the (real) effective permittivity [2,8,27,38,39,45,46], let us further consider that the polycrystal is isotropic in the sense that $\langle \mathbf{e}_1^T \mathbf{R} \mathbf{e}_1 \rangle = \langle \mathbf{e}_2^T \mathbf{R} \mathbf{e}_2 \rangle = \langle \mathbf{e}_3^T \mathbf{R} \mathbf{e}_3 \rangle$. Then $\langle \mathbf{e}_k^T \mathbf{R} \mathbf{e}_k \rangle = 1/2$ in two dimensions and $\langle \mathbf{e}_k^T \mathbf{R} \mathbf{e}_k \rangle = 1/3$ in three dimensions. Here, our upper bound is in agreement with the upper bound presented in [2] for a uniaxial isotropic polycrystal. However, our lower bound is in disagreement with the lower bound presented in [2] for a uniaxial isotropic polycrystal. A quick argument can justify the difference. The lower bound in Avellaneda *et al.* [2] is achieved with the *sphere assemblage model* conjectured by Schulgasser [45,46]. The reason being that the conductivity in each direction is simultaneously minimized in the equation $\epsilon^* = (1/3)tr(\epsilon^*) \geq \epsilon_s$ [2], where ϵ_s is the permittivity of the *sphere assemblage model* and ϵ^* is the full permittivity tensor. Therefore, a minimum is found and achieved with the *sphere assemblage model* because all directions have the same minimum permittivity. The lower bound we find here is only for $\langle \mathbf{e}_k^T \mathbf{R} \mathbf{e}_k \rangle$ the same in each direction, not necessarily the permittivity to be the same. Thus, in a single direction, the minimum value that can be obtained is still the harmonic bound (i.e., resistors in series). Using a nearly identical argument, there is also no reason for these lower bounds to be the same in the anisotropic case. The bounds we find here are needed to examine sea ice because we are interested in the effective complex permittivity for a single direction.

3. Inverse Bounds for Structural Parameters

The objective of inverse bounds is to use data from the electromagnetic response of a polycrystalline material to recover information about its structural parameters. In previous work [9], this is typically done to recover information about the volume fractions of the two constituents of a composite material. Here, we will show how to recover information about the mean crystal orientation $\langle \mathbf{e}_k^T \mathbf{R} \mathbf{e}_k \rangle$ of the polycrystalline material. The inverse method [9,21,33,34] we use here yields intervals of uncertainty for the mean crystal orientation $\langle \mathbf{e}_k^T \mathbf{R} \mathbf{e}_k \rangle$. Given an observed value of the complex permittivity in a single direction ϵ^* , $\langle \mathbf{e}_k^T \mathbf{R} \mathbf{e}_k \rangle$ is increased until the value of ϵ^* touches one boundary of the region R_3 described in the previous section, and is then decreased until the value touches the other boundary. This procedure gives a range of values $\langle \mathbf{e}_k^T \mathbf{R} \mathbf{e}_k \rangle_l \leq \langle \mathbf{e}_k^T \mathbf{R} \mathbf{e}_k \rangle \leq \langle \mathbf{e}_k^T \mathbf{R} \mathbf{e}_k \rangle_u$, with

$$\langle \mathbf{e}_k^T \mathbf{R} \mathbf{e}_k \rangle_l = |f|^2 \frac{Im(\bar{s})}{Im(f)}, \quad \langle \mathbf{e}_k^T \mathbf{R} \mathbf{e}_k \rangle_u = 1 - \frac{|g|^2 Im(\bar{t})}{Im(g)}, \quad (3.1)$$

where f is the known value of $F(s)$ and g is the known value of $G(t) = 1 - \epsilon^*/\epsilon_1$ with $t = 1 - s$.

The objective of the second order inverse bounds would be to obtain a better estimate for the mean orientation of crystals in the k th direction. However, as demonstrated in the second order forward bounds, the mean orientation must be the same in all directions. Thus we already know that, $\langle \mathbf{e}_k^T \mathbf{R} \mathbf{e}_k \rangle = 1/d$ and therefore, the second order inverse bounds provide no new information or are essentially meaningless for polycrystalline composites.

4. Comparison of the Bounds to Sea Ice Data

Here the polycrystalline bounds are compared with the data set in [1], which is obtained from primarily columnar sea ice. This data set is the same as was used to compare sea ice with the elementary bounds of a two-component material [9,16], a statistically isotropic two-component material [9,16], and a two-component matrix-particle material [40,44]. Applying the polycrystalline bounds to this same set of data allows for comparison between different types of bounds and hopefully allows for a deeper understanding of the physical relationship the polycrystalline bounds have to sea ice data. In addition, this is the only known data set (to our knowledge) that is accompanied by a detailed analysis of the crystalline structure of the ice, which is necessary for the polycrystalline bounds to be applied. To obtain forward bounds and compare them with sea ice data, two things must be known: the complex permittivity tensor of the identical single crystals (i.e., ϵ_1 and ϵ_2), and the crystal orientation statistics (i.e., $\langle \mathbf{e}_k^T \mathbf{R} \mathbf{e}_k \rangle$).

The single crystal complex permittivity tensor for sea ice is obtained by evaluating X-ray CT data with known ice and brine permittivities and ϕ using Comsol 3.5a. Here we examine 222 single crystals at a frequency of 4.75 GHz and at a temperature of -6°C , where brine has a permittivity value of $51.0741 + i45.1602$ [51]. As was demonstrated in [9], it is important not to neglect the effect of the air phase of sea ice when calculating the complex permittivity. Thus, to account for this air phase, a Maxwell-Garnett mixing formula is used apriori to combine the air and ice phase as was done identically in [9]. Therefore, the permittivity used for the air-ice phase is $3.07 + i0.0019$. Different single crystal microstructures were calculated at different ϕ values and a data set of single crystal complex permittivity tensors was generated (Table 1).

Different sea ice single crystal geometric configurations can have significantly different permittivity tensors for the same brine volume fraction ϕ value as is shown in Table 1. In particular, the permittivity in the vertical direction can dramatically change depending on the brine connectedness in the vertical direction. Additionally, the two horizontal components tend to have slightly different permittivity values. The polycrystalline bounds make the assumption that the material is composed of many identical crystals with the same permittivity in two directions (transversely isotropic or uniaxial) and a different permittivity in the other (vertical) direction. As is quickly observed in Table 1 actual sea ice directly violates these assumptions, namely that each crystal is identical and the horizontal permittivities are the same. To make matters worse, ϕ values can dramatically change across an entire sea ice column, thus substantially changing the single crystal permittivities at different depths. For example, the very bottom layer of a sea ice column can have a ϕ value almost twice as large as the average, which is typical in classic columnar sea ice [13,57]. Further, as displayed in Table 1, the permittivity change in the vertical component is not linear with respect to ϕ , and a “small range” general average in the vertical direction for a specific ϕ value will not accurately represent the physics of the ice. To account for these differences between the requirements for the polycrystalline bounds and actual sea ice data, we will “idealize” the sea ice data, so that the polycrystalline bounds may still be applied. Inherently, this “idealization” changes the objective from finding an exact forward bound for a very specific configuration with identical single crystals to finding a more general forward bound that can be applied to a large class of sea ice, such as all columnar sea ice within a certain ϕ value range. Thus, to obtain the single crystal permittivity tensor for ϕ corresponding to the entire ice column, we averaged the permittivities in the vertical direction and both of the horizontal directions over a range of ϕ , accounting for a typical variation in ϕ across an entire ice column. For example, for an average value of $\phi = 3.5\%$ we used the following range of (averaged) ϕ values: 0.025, 0.025, 0.025, 0.03, and 0.07. For an average value of $\phi = 4\%$, we used the following range of (averaged) ϕ values: 0.03, 0.03, 0.03, 0.03, 0.04, and 0.08. Therefore, the single crystal permittivity tensor for an entire column of sea ice with overall values of $\phi = 3.5\%$ and $\phi = 4\%$ are: $\epsilon_1 = 3.74 + 0.62i$ (vertical), $\epsilon_2 = 3.46 + 0.08i$ (horizontal), and $\epsilon_1 = 4.11 + 0.67i$ (vertical), $\epsilon_2 = 3.52 + 0.10i$ (horizontal), respectively.

The polycrystalline forward bounds also assume that we know the single crystal orientation statistics $\langle \mathbf{e}_k^T \mathbf{R} \mathbf{e}_k \rangle$. Here we use the orientation statistics found in [56]. These data describe the

c-axis distribution statistics of sea ice as a function of depth for ice grown in a region without a preferred current direction (thus, transversely isotropic). The big picture is that granular ice (typically found in the top layer of a column of sea ice [56]) has an essentially random uniform distribution across all angles, whereas columnar ice has a strongly preferred vertical orientation. The effective complex permittivity data set from [1] is largely columnar and cross-sectional slices show that the sea ice is transversely isotropic. Examining the orientation statistics [56], it is very reasonable to conclude that the average crystal orientation $\langle \mathbf{e}_k^T \mathbf{R} \mathbf{e}_k \rangle$ for the largely columnar ice structure used in [1] has average orientation measurements somewhere between 0 degrees and 30 degrees off the vertical axis.

Due to the necessary “idealizations” as describe above, the objective of the forward bounds is to capture all possible effective complex permittivity variations that can occur in columnar ice. The electromagnetic wave propagating through the sea ice column in [1] is orthogonal to the horizontal plane, thus the electric field is in the horizontal plane. The horizontal plane is isotropic, therefore, we can just examine one of the horizontal directions (depending on which direction you assume the electric field is in) and use a two-dimensional rotation matrix, which would give the same result as a three-dimensional rotation matrix where the electric field is in exactly one of the horizontal directions. Therefore, if we say the electric field is in the $k=2$ horizontal direction, and for an average orientation between 0 and 30 degrees off the vertical axis (i.e., columnar ice) $\langle \mathbf{e}_2^T \mathbf{R} \mathbf{e}_2 \rangle$ takes a value between $\sin^2(0) = 0$ and $\sin^2(30) = 0.25$. For primarily granular ice, the average crystal orientation statistics are very uniform over the possible range of angles and the average angle should be close to 45 degrees. An acceptable range might be between 35 and 55 degrees. We are unaware of any experiments that have taken permittivity data for primarily granular ice and therefore we unfortunately have no data with which to compare these bounds.

The first order polycrystalline forward bounds can then be applied to the data and the largest area of overlap between the bounds is assumed to be the region where the data must lie. It is possible that the forward bounds overestimate the region because of this technique (namely, we assume the mean orientation is between 0 and 30 degrees off the vertical axis). However, each region in these bounds could still be found by slightly adjusting the single crystal permittivity tensor (which can have some variability) for a specific orientation. Further, it is also certainly reasonable to use this approach because of the large (and possibly unknown) variability in the general columnar crystal orientation statistics from sample to sample. Essentially, these bounds are general enough that they can be applied accurately to all sea ice that is primarily columnar without having to know specific orientation statistics or a specific single crystal permittivity tensor. The second order forward bounds cannot be compared to this sea ice data because they assume that the material is geometrically isotropic. This is not the case for columnar sea ice. We mention them here because on occasion the second order forward bounds might be applicable to granular ice, but as mentioned above we have no granular data to examine.

As displayed in Figure 1 (a) the polycrystalline bounds provide a much tighter bound than those of the traditional two-component material and statistically isotropic two-component material for sea ice. This makes sense because we are essentially applying a two-scale homogenization and including the additional information about rotation statistics. If we zoom in on just the new polycrystalline bounds, we see that the bounds accurately capture the data for the corresponding ϕ value for the ice column (Figure 2 (a)), minus one point. We suspect that this missing point can easily be justified by the variability in single crystal permittivities. However, we suggest that the three tighter bounds in Figure 1 (a) and the bounds in Figure 2 (a) be viewed as a “window” for whole column, columnar sea ice permittivities where brine volume fractions vary between $3.3\% \leq \phi \leq 4.1\%$.

Although the bounds accurately capture the data, due the large variability and potential noise in both the data in [1] and the single crystal permittivity tensor from our numerical simulations, we further average the data in [1] and compare it to bounds corresponding to the single crystal permittivity tensor of the averaged value of $\phi = 3.75\%$. This is displayed in Figure 1 (b) and Figure 2 (b), and we see that the bounds accurately capture the data point.

We further examine the data under the inverse polycrystalline bounds. For the data falling within a certain ϕ value range (thus we know the single crystal permittivity tensor), we can estimate the mean crystal orientation, revealing the type of ice. The results are displayed in Figure 3. Namely, we estimate that the mean crystal orientation of the ice crystals in the ice column from the Arcone *et al.* experiments is between 8 and 30 degrees off the vertical axis. Therefore, the ice is certainly columnar. If we then examine two images from [1] that are representative of the typical sea ice structure from which the complex permittivity data was taken, and then estimate the mean crystal orientation, we estimate that the average crystal orientation should be somewhere between 11.5 and 19 degrees off the vertical axis. These are within the inverse bounds mean single crystal orientation range displayed in Figure 3.

5. Figures & Tables

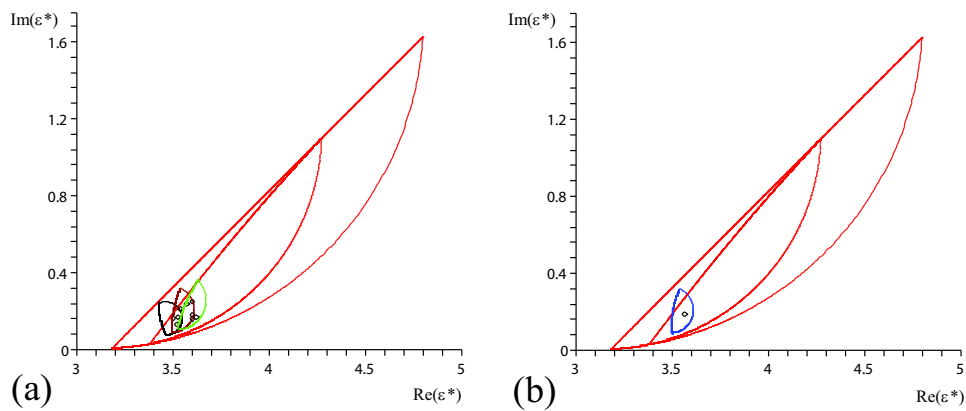


Figure 1. Comparison of previous and new forward bounds with complex permittivity data. **(a)** Forward elementary bounds and isotropic bounds for a two component material are red [9,16]. The forward polycrystalline bounds for columnar sea ice where the single crystal permittivity tensor has a brine volume fraction of 4% are green, 3.75% are brown, and 3.5% are black. These data points correspond to complex permittivity data taken at 4.75 GHz and where the brine volume fraction approximately spans between 3.1% and 4.1%. **(b)** Forward elementary bounds and isotropic bounds for a two component material are again red [9,16]. The forward polycrystalline bounds for columnar sea ice where the single crystal permittivity tensor has a brine volume fraction of 3.75% is blue compared with the averaged effective complex permittivity data taken at 4.75 GHz where the averaged brine volume fraction is 3.65%.

6. Conclusion

We have developed both first and second order forward bounds on the effective complex permittivity ϵ^* for a polycrystalline material using the analytic continuation method. Additionally, we have obtained first order inverse bounds on the mean single crystal orientation for a polycrystalline material. The first order forward bounds assume a priori knowledge about the complex permittivity tensor for a single crystal and the mean single crystal orientation, and bound ϵ^* . The second order polycrystalline forward bounds further require that the material is geometrically isotropic in the polycrystalline Hashin-Shtrikman sense. The inverse bounds for the polycrystalline material assume knowledge about ϵ^* and the complex permittivity tensor for a single crystal and bound the mean crystal orientation. We further compare these bounds

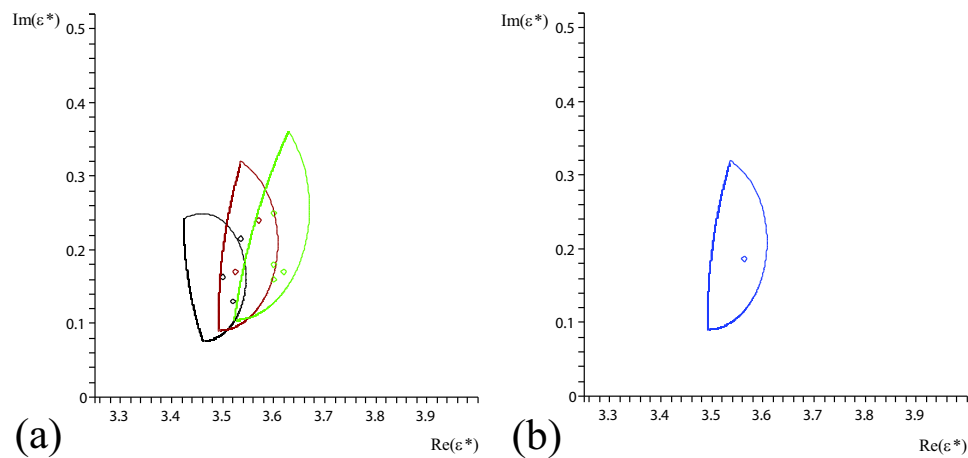


Figure 2. Comparison of new forward bounds with complex permittivity data. **(a)** “Zoomed-in” version of Figure 1 (a) displaying the forward polycrystalline bounds for columnar sea ice where the single crystal permittivity tensor has a brine volume fraction of 4% (green), 3.75% (brown), and 3.5% (black), compared with effective complex permittivity data taken at 4.75 GHz where the averaged brine volume fraction is 4% (green), 3.65% (brown), and 3.33% (black). The brown data point that is capture by both the black and brown bounds is used in both (black and brown) data averages. Note how multiple data points fall within multiple bounds. **(b)** “Zoomed-in” version of Figure 1 (b) displaying the forward polycrystalline bounds for columnar sea ice where the single crystal permittivity tensor has a brine volume fraction of 3.75% (blue), compared with the averaged effective complex permittivity data taken at 4.75 GHz where the averaged brine volume fraction is 3.65% (blue).

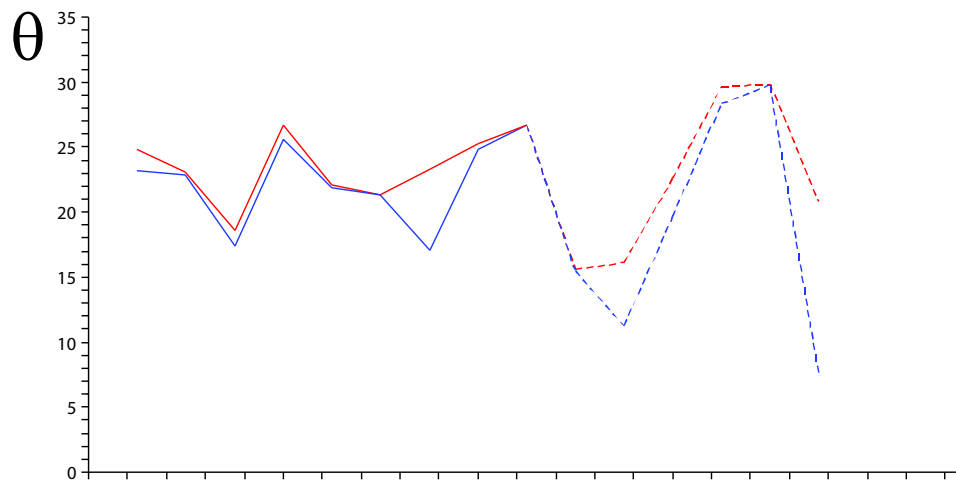


Figure 3. Inverse bounds on the mean crystal orientation off the vertical axis (y-axis) for 15 different effective complex permittivity data values (x-axis). The dashed line represents data points that were examined for the secondary forward bound they fell within. Here we see the upper inverse bounds (red) and lower inverse bounds (blue) for the 15 different data values.

Table 1. A sample of the range of complex permittivity values that a single crystal of sea ice can display. Note that at a constant brine volume fraction ϕ of 3.8% and 5.5%, the values of the vertical component can dramatically change. Also note that the vertical component does not change on a linear scale with an increase in ϕ . This data was generated from numerical simulations of X-ray CT sea ice microstructures using Comsol 3.5a.

| BVF | Vertical Component | Horizontal component 1 | Horizontal component 2 |
|-------|--------------------|------------------------|------------------------|
| 0.025 | 3.4796+0.0795027i | 3.34554+0.0386595i | 3.2315+0.0150707i |
| 0.03 | 3.90874+0.376569i | 3.32704+0.030911i | 3.44001+0.0919011i |
| 0.038 | 3.62198+0.112947i | 3.49521+0.0687332i | 3.52569+0.0947335i |
| 0.038 | 3.79782+0.211531i | 3.36183+0.0325894i | 3.55585+0.0885505i |
| 0.038 | 3.88906+0.345808i | 3.36387+0.0336083i | 3.73552+0.192388i |
| 0.055 | 4.93418+1.45498i | 3.43891+0.0454075i | 3.71922+0.103182i |
| 0.055 | 4.14111+0.267123i | 3.63189+0.107398i | 3.60756+0.0749424i |
| 0.055 | 4.33091+0.425696i | 3.49575+0.0485316i | 3.76794+0.149307i |
| 0.081 | 6.53291+3.16979i | 3.46572+0.0267835i | 4.3584+0.256975i |
| 0.124 | 7.8748+4.23181i | 3.82923+0.0618386i | 4.77605+0.30978i |

with actual sea ice data and find excellent agreement. These results provide a foundation for determining ice type with remote sensing techniques.

Acknowledgments

We gratefully acknowledge support from the Division of Mathematical Sciences and the Division of Polar Programs at the U.S. National Science Foundation (NSF) through Grants DMS-1009704, ARC-0934721, DMS-0940249, and DMS-0602219. We are also grateful for support from the Office of Naval Research (ONR) through Grant N00014-13-10291. Finally, we would like to thank the NSF Math Climate Research Network (MCRN) for their support of this work.

References

1. S. A. Arcone, A. J. Gow, and S. McGrew.
Structure and dielectric properties at 4.8 and 9.5 GHz of saline ice.
J. Geophys. Res., 91(C12):14281–14303, 1986.
2. M. Avellaneda, A. V. Cherkaev, K. A. Lurie, and G. W. Milton.
On the effective conductivity of polycrystals and a three-dimensional phase interchange inequality.
J. Appl. Phys., 63:4989, doi:10.1063/1.340445, 1988.
3. S. Barabash and D. Stroud.
Spectral representation for the effective macroscopic response of a polycrystal: application to third-order non-linear susceptibility.
J. Phys. Condens. Matter, page 10323, 1999.
4. D. J. Bergman.
The dielectric constant of a composite material – A problem in classical physics.
Phys. Rep. C, 43(9):377–407, 1978.
5. D. J. Bergman.
Exactly solvable microscopic geometries and rigorous bounds for the complex dielectric constant of a two-component composite material.
Phys. Rev. Lett., 44:1285, 1980.
6. D. J. Bergman.
Rigorous bounds for the complex dielectric constant of a two-component composite.
Ann. Phys., 138:78, 1982.
7. F. D. Carsey, editor.
Microwave Remote Sensing of Sea Ice, Geophysical Monograph 68.

- American Geophysical Union, Washington D.C., 1992.
8. A. Cherkaev.
Variational Methods for Structural Optimization, volume 140 of *Applied Mathematical Sciences*. Springer-Verlag, New York, 2000.
 9. E. Cherkaeva and K. M. Golden.
Inverse bounds for microstructural parameters of composite media derived from complex permittivity measurements.
Waves in Random Media, 8(4):437–450, 1998.
 10. E. Cherkaeva and A. C. Tripp.
Bounds on porosity for dielectric logging.
In *European Consortium for Mathematics in Industry 96*, pages 304–306. Danish Technical University, 1996.
 11. P. D. Chinh.
Bounds on the effective conductivity of statistically isotropic multicomponent materials and random cell polycrystals.
J. Mech. Phys. Sol., 59:497, 2011.
 12. K. E. Clark.
A continued fraction representation for the effective conductivity of a two-dimensional polycrystal.
J. Math. Phys., 38:4528, doi:10.1063/1.532141, 1997.
 13. H. Eicken.
Growth, microstructure and properties of sea ice.
In D. N. Thomas and G. S. Dieckmann, editors, *Sea Ice: An Introduction to its Physics, Chemistry, Biology and Geology*, pages 22–81. Blackwell, Oxford, 2003.
 14. H. Eicken, T. C. Grenfell, D. K. Perovich, J. A. Richter-Menge, and K. Frey.
Hydraulic controls of summer Arctic pack ice albedo.
J. Geophys. Res. (Oceans), 109(C18):C08007.1–C08007.12, 2004.
 15. C. H. Fritsen, V. I. Lytle, S. F. Ackley, and C. W. Sullivan.
Autumn bloom of Antarctic pack-ice algae.
Science, 266:782–784, 1994.
 16. K. Golden.
Bounds on the complex permittivity of sea ice.
J. Geophys. Res. (Oceans), 100(C7):13,699 – 13,711, 1995.
 17. K. Golden and G. Papanicolaou.
Bounds for effective parameters of heterogeneous media by analytic continuation.
Comm. Math. Phys., 90:473–491, 1983.
 18. K. Golden and G. Papanicolaou.
Bounds for effective parameters of multicomponent media by analytic continuation.
J. Stat. Phys., 40(5/6):655–667, 1985.
 19. K. M. Golden.
The interaction of microwaves with sea ice.
In G. Papanicolaou, editor, *Wave Propagation in Complex Media, IMA Volumes in Mathematics and its Applications*, Vol. 96, pages 75 – 94. Springer – Verlag, 1997.
 20. K. M. Golden and S. F. Ackley.
Modeling of anisotropic electromagnetic reflection from sea ice.
J. Geophys. Res. (Oceans), 86(C9):8107–8116, 1981.
 21. K. M. Golden, D. Borup, M. Cheney, E. cherkaev, M. S. Dawson, K. H. Ding, A. K. Fung, D. Isaacson, S. A. Johnson, , A. K. Jordan, J. A. Kong, R. Kwok, S. V. Nghiem, R. G. Onstott, J. Sylvester, D. P. Winebrenner, and I. Zabel.
Inverse electromagnetic scattering models for sea ice.
IEEE Trans. Geosci. Rem. Sens., 36(5):1675–1704, 1998.
 22. K. M. Golden, M. Cheney, K. H. Ding, A. K. Fung, T. C. Grenfell, D. Isaacson, J. A. Kong, S. V. Nghiem, J. Sylvester, and D. P. Winebrenner.
Forward electromagnetic scattering models for sea ice.
IEEE Trans. Geosci. Rem. Sens., 36(5):1655–1674, 1998.
 23. K. M. Golden, A. Gully, C. S. Sampson, D. J. Lubbers, and J. L. Tison.
Percolation threshold for fluid permeability in Antarctic granular sea ice.
In preparation, 2014.

24. A. Gully, L.G.E. Backstrom, H. Eicken, and K.M. Golden.
Complex bounds and microstructural recovery from measurements of sea ice permittivity.
Physica B, 394:357, 2007.
25. Z. Hashin and S. Shtrikman.
A variational approach to the theory of effective magnetic permeability of multiphase materials.
J. Appl. Phys., 33:3125–3131, 1962.
26. Z. Hashin and S. Shtrikman.
Conductivity of polycrystals.
Phys. Rev., 130:129–133, 1963.
27. J. Helsing.
Improved bounds on the conductivity of composites by interpolation.
Proc. R. Soc. London A, 444:363–374, 1994b.
28. M. O. Jeffries, editor.
Antarctic Sea Ice: Physical processes, interactions and variability.
American Geophysical Union, Washington D.C., 1998.
29. M. P. Lizotte and K. R. Arrigo, editors.
Antarctic Sea Ice: Biological processes, interactions and variability.
American Geophysical Union, Washington D.C., 1998.
30. D. Lubin and R. Massom.
Polar Remote Sensing, Volume I: Atmosphere and Oceans.
Springer Verlag, New York, 2006.
31. V. I. Lytle and S. F. Ackley.
Heat flux through sea ice in the Western Weddell Sea: Convective and conductive transfer processes.
J. Geophys. Res., 101(C4):8853–8868, 1996.
32. T. Maksym and T. Markus.
Antarctic sea ice thickness and snow-to-ice conversion from atmospheric reanalysis and passive microwave snow depth.
J. Geophys. Res., 113:C02S12, doi:10.1029/2006JC004085, 2008.
33. R. C. McPhedran, D. R. McKenzie, and G. W. Milton.
Extraction of structural information from measured transport properties of composites.
Appl. Phys. A, 29:19–27, 1982.
34. R. C. McPhedran and G. W. Milton.
Inverse transport problems for composite media.
Mat. Res. Soc. Symp. Proc., 195:257–274, 1990.
35. G. W. Milton.
Bounds on the complex dielectric constant of a composite material.
Appl. Phys. Lett., 37:300–302, 1980.
36. G. W. Milton.
Bounds on the complex permittivity of a two-component composite material.
J. Appl. Phys., 52:5286–5293, 1981.
37. G. W. Milton.
Bounds on the transport and optical properties of a two-component composite material.
J. Appl. Phys., 52:5294–5304, 1981.
38. G. W. Milton.
Theory of Composites.
Cambridge University Press, Cambridge, 2002.
39. V. Nesi and G. W. Milton.
Polycrystalline configurations that maximize electrical resistivity.
J. Mech. Phys. Sol., 39:525, 1991.
40. C. Orum, E. Cherkaev, and K. M. Golden.
Recovery of inclusion separations in strongly heterogeneous composites from effective property measurements.
Proc. Royal Soc. Series A, 468:784–809, 2012.
41. D. K. Perovich, B. Light, H. Eicken, K. F. Jones, K. Runciman, and S. V. Nghiem.
Increasing solar heating of the Arctic Ocean and adjacent seas, 1979–2005: Attribution and role in the ice-albedo feedback.

- Geophys. Res. Lett.*, 34:L19505, doi:10.1029/2007GL031480, 2007.
42. J. E. Reid, A. P. Worby, J. Vrbancich, and A. I. S. Munro.
Shipborne electromagnetic measurements of Antarctic sea-ice thickness.
Geophysics, 68(5):1537–1546, 2003.
 43. S. Rysgaard, R. N. Glud, M. K. Sejr, J. Bendtsen, and P. B. Christensen.
Inorganic carbon transport during sea ice growth and decay: A carbon pump in polar seas.
J. Geophys. Res., 112:C03016, doi:10.1029/2006JC003572, 2007.
 44. R. Sawicz and K. Golden.
Bounds on the complex permittivity of matrix-particle composites.
J. Appl. Phys., 78:7240–7246, 1995.
 45. K. Schulgasser.
Bounds on the conductivity of statistically isotropic polycrystals.
J. Phys. C, 10:407, 1977.
 46. K. Schulgasser.
Sphere assemblage model for polycrystals and symmetric materials.
J. Appl. Phys., 54:1380, doi:10.1063/1.332161, 1983.
 47. M. C. Serreze, M. M. Holland, and J. Stroeve.
Perspectives on the Arctic's shrinking sea-ice cover.
Science, 315:1533–1536, 2007.
 48. R. A. Shuchman and R. G. Onstott.
Remote sensing of the polar oceans.
In W. O. Smith, editor, *Polar Oceanography, Part A, Physical Science*, pages 123–169. Academic Press, 1990.
 49. A. H. Sihvola and J. A. Kong.
Effective permittivity of dielectric mixtures.
IEEE Trans. Geosci. Remote Sensing, 26(4):420–429, 1988.
 50. A. Stogryn.
An analysis of the tensor dielectric constant of sea ice at microwave frequencies.
IEEE Trans. Geosci. Remote Sensing, GE-25(2):147–158, 1985.
 51. A. Stogryn and G. J. Desargant.
The dielectric properties of brine in sea ice at microwave frequencies.
IEEE Trans. Antennas Propagat., AP-33(5):523–532, 1985.
 52. D. N. Thomas and G. S. Dieckmann, editors.
Sea Ice, Second Edition.
Wiley-Blackwell, Oxford, 2009.
 53. A. C. Tripp, E. cherkaev, and J. Hulen.
Bounds on the complex conductivity of geophysical mixtures.
Geophysical Prospecting, in press.
 54. N. Untersteiner.
Some problems of sea ice and climate modelling.
Verhöff. Univ. Innsbruck, 178:209–228, 1990.
 55. M. R. Vant, R. O. Ramseier, and V. Makios.
The complex-dielectric constant of sea ice at frequencies in the range 0.1–40 GHz.
J. Appl. Phys., 49(3):1264–1280, 1978.
 56. W. F. Weeks and S. F. Ackley.
The growth, structure and properties of sea ice.
CRREL Monograph 82-1, page 130 pp., 1982.
 57. W. F. Weeks and S. F. Ackley.
The growth, structure and properties of sea ice.
In N. Untersteiner, editor, *The Geophysics of Sea Ice*, pages 9–164. Plenum Press, New York, 1986.
 58. D. P. Winebrenner, J. Bredow, A. K. Fung, M. R. Drinkwater, S. Nghiem, A. J. Gow, D. K. Perovich, T. C. Grenfell, H. C. Han, J. A. Kong, J. K. Lee, S. Mudaliar, R. G. Onstott, L. Tsang, and R. D. West.
Microwave sea ice signature modeling.
In F. D. Carsey, editor, *Microwave Remote Sensing of Sea Ice, Geophysical Monograph 68*, pages 137–175. American Geophysical Union, 1992.